10TH INTERNATIONAL SYMPOSIUM ON PARTICLE IMAGE VELOCIMETRY - PIV13
Delft, The Netherlands, July 1-3, 2013

Tomographic particle-image velocimetry in an IC engine

Timo van Overbrüggen[1], Björn Bahl[1], Uwe Dierksheide[2], Michael Klaas[1], Wolfgang Schröder[1]

[1] Institute of Aerodynamics, RWTH Aachen, University, Aachen, Germany, t.van-overbrueggen@aia.rwth-aachen.de

[2] LaVision GmbH, Anna-Vandenhoeck-Ring 19, Göttingen, Germany

ABSTRACT

The flow structures during the intake and compression phase within the cylinder of an internal combustion(IC)engine strongly influence the mixing and combustion process. To gain a better understanding of the flow field, fully three-dimensional quantitative measurement techniques have to be applied to the flow field. Analog off-axis holographic particle-image velocimetry is capable of resolving the whole flow field of an IC engine with very high resolution (van Overbrueggen et. al [21]). On the other hand, long processing procedures make this technique not feasible for a statistic flow field analysis. Tomographic particle-image velocimetry (Tomo-PIV) is another three-component/three-dimensional (3C/3D) measurement technique that could be used. It is digital and therefore possesses the advantage of relatively short processing time. In this study, cycle resolved tomographic particle-image velocimetry measurements are performed in a four-valve IC engine to resolve the highly three dimensional flow in a large area of the cylinder. The resolved volume has a size of about 60 x 60 x 80 mm^3 for the 160° measurements. The three-dimensional structure of the flow field is analyzed for 80°, 160°, and 240° after top dead center (aTDC) during the intake and compression phase at an engine speed of 1,500 rpm. The flow fields are analyzed by ensemble-averaged velocity fields, turbulent kinetic energy (TKE), and the Γ_1 vortex center criterion. The results provide detailed inside in the highly three-dimensional flow field inside an internal combustion engine and show the feasibility of tomographic PIV to resolve such a large volume in a complex geometry.

1. INTRODUCTION

Increasing fuel prices, as well as global warming, and hence the discussion about pollutant emissions like nitrogen dioxide (NO_x), carbon dioxide (CO_2), and soot generates an interest in the reduction of tuel consumption in internal combustion (IC) engines. Therefore, a focus point of engine developement are new combustion processes that both decrease fuel consumption and increas the power output of the engine. Here, the so-called Controlled Auto-Ignition (CAI) and the Homogeneous Charge Compression Ignition (HCCI) play a prominent role in modern engine development. Both are characterized by a high homogenization and exhaust gas recirculation (EGR). Homogenization avoids partial combustion such that soot emission decreases, whereas lower combustion temperatures significantly reduce NO_x emissions. The lower combustion temperatures are achieved through the high thermal heat capacity of the recirculated exhaust gas. Due to dethrottling of CAI engines and a faster combustion near the top dead center (TDC), fuel consumption is reduced. Lang et al. [11] reported a maximum fuel reduction of 15% and a reduction of NO_x emissions by up to 90 - 99 %. Unfortunately, knocking and misfireing both limit the operating range of CAI as well as HCCI (Ma et al. [12], Urushihara [20], Bhave et al. [3]). These instabilities cannot be controlled by combustion performance measures, e.g., air-fuel ratio measurements. Therefore, a controler has to supress the instabilities on a physical and chemical basis. Stapf et al. [18] state that self-ignition highly depends on the stratification of fuel, EGR, and fresh air. Consequently, the control of the combustion process strongly depends on the thermodynamic conditions of the in-cylinder mixture (Adomeit et al. [1]). These conditions are highly dependant on the flow within the cylinder especially during intake and compression stroke.Thus, a detailed analysis of the temporal and spatial development of the characteristic flow phenomena during these crank angles helps to gain a better understanding of the mixing process.

Two-component planar PIV (2D/2C) can be considered state-of-the-art for all kinds of applications, including engines. One horizontal and two vertical planes within the cylinder were measured by Reeves et al. [14]. The angular momentum around a specific axis in the combustion chamber for different engine speeds were analized by Stansfield et al. [17]. They found a significant change of the fundamental flow between 2,500 and 3,000 rpm. Dannemann et al. [8] performed planar PIV measurements for several crank angles in an unfired one-cylinder four-valve IC engine. They analyzed the three-dimensional structure of the velocity field based on flow field measurements in eight axial planes. The quasi three-dimensional flow field was reconstructed from the two-dimensional velocity fields for crank angles of 80, 160, and 240 after top dead center (aTDC). Furthermore, the propagation of the flow field between crank angles of 40 and 320 aTDC in steps of 20 was discussed for both symmetry planes. The authors showed that the flow inside an IC engine possesses a highly three-dimensional character. Furthermore, large vortical structures, e.g., ring vortices beneath the inlet valves and their temporal development could be shown. To resolve all three velocity components in one plane, stereoscopic PIV measurements were first performed in an IC engine by Calendini et al. [7]. They recorded 35 double images in the center plane between inlet and outle valves for different crank angles at 1,000 rpm. However, the ensemble averaged measurements were not able to visualize large scale structures like ring vortices or the tumble vortex. Bücker et al. [5, 6] performed stereoscopic PIV measurements in a set of planes for several crank angles at 1,500 rpm. They visualized large scale structures and analyzed the temporal development of the mean kinetic energy in two measurement planes. However, the highly three-dimensional structure of the flow requires the application of a three-component volumetric or quasi-volumetric measurement technique to instantaneously capture all three velocity components in the complete cylinder.

First quasi-volumetric measurements in an internal combustion engine were performed via holographic PIV by Konrath et al. [10],

who performed holographic PIV measurements in two parallel planes simultaneously with high spatial resolution. First fully three-dimenasional holographic PIV measurements were performed by van Overbrüggen et al. [21] who measured three instantaneous flow fields at 160° aTDC in a large volume with high resolution. First tomographic PIV measurements were performed by Baum et al. [2] for two crank angles in a volume with a depth of field of 4 mm and 8 mm. In this study, the instantaneous three-dimensional velocity field is measured at 80, 160, and 240 after top dead center (aTDC) by tomographic PIV to show the feasibility of the measurement technique and to gain information of the spatial distribution of the large and small scale structures of the in-cylinder flow.
The article is organized as follows. First, the optical four-valve research engine is described in detail. Then, the tomographic PIV setup as well as the processing procedure are explained. This is followed by a description of the used seeding material. The discussion of the results starts with an error estimation. Subsequently, the three-dimensional volumetric flow fields of the three measurement points are explained in detail.

2. EXPERIMENTAL SETUP

2.1 Optical engine

The research engine is a modified Suzuki DR750 motorcycle four-stroke four-valve single-cylinder IC engine. It is driven by an electrical 55kW engine, i.e., the engine is not fired. The bore of the engine is D = 105 mm and the stroke is 85 mm with a resulting cylinder displacement of V = 728 cm^3. The original cylinder of the Suzuki engine has been replaced by a transparent Perspex liner to grant optical access to the in-cylinder flow. The optical cylinder is placed between the original cylinder head of pent roof geometry and an elongated lower liner, that keeps the piston properly aligned. Free piston movement within the optical liner is ensured, due to a clearance between piston and liner of 0.16 mm. The larger top-land crevice volume reduces the the engine compression rate from 9.5 to 9. To get an undisturbed view of the flow, the camshaft drive chain was replaced by means of an elongated camshaft and crankshaft. The flat piston crown also consists of Perspex to ensure optical access. The engine is operated at a mean revolution speed of 1,500 rpm without fuel injection and combustion. The typical progression of the engine speed n, showing the decay due to compression, the piston speed, and the valve lift of the inlet and exhaust valves are plotted in fig. 2. The red lines mark the measurement points. To avoid a critical temperatur of the Perspex liner, the engine can only be operated for about $t < 120$ s. A shaft encoder at a resolution of 1 provides the crank angle and can be used to measure the engine speed. Due to the four-stroke cycle length of 720, a reflective sensor scans a coding disk mounted to the camshaft to clearly identify intake, compression, power, and exhaust stroke (fig. 1. The seeding particles for PIV measurements are provided through an additional reservoir connected to the cylinder intake port. Two flaps in front of the intake ports of the cylinder head allow a fast switching between seeded and unseeded air to minimize the particle contamination of the optical liner during the engine start process (Konrath et al. [10]). A few cycles before the PIV images are recorded, the flaps are released to provide seeded air for the measurements.

2.2 Tomographic Particle-Image Velocimetry system

The tomographic PIV system consists of two Spitlight 600 single-cavity Nd:YAG lasers with a maximum output power of about 400 mJ per pulse, four sCMOS cameras (PCO edge, 2560 x 2160 pixels, 16-bit, double-frame exposure), and Zeiss lenses with a focal length of 100 mm. The cameras were arranged horizontally in a circular area around the center axis of the cylinder. This ensures a similar distortion for all four cameras. The angle between camera 1 and camera 4 is $\alpha = 75°$, the angle between camera 2 and camera 3 is $\beta = 36°$ (fig 3). Scheimpflug adpaters and an aperture of f/22 and a magnification of $M_0 = 0.18$ were used, providing a depth-of-field of 64 mm. Due to the radial distortion

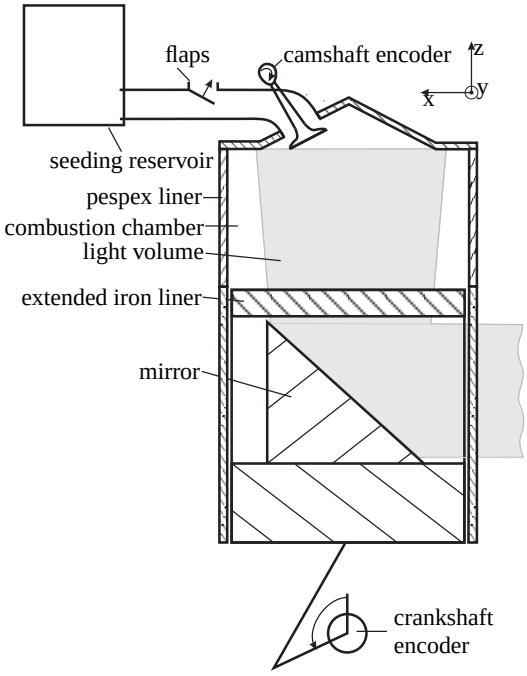

Figure 1: Schematic of the test engine

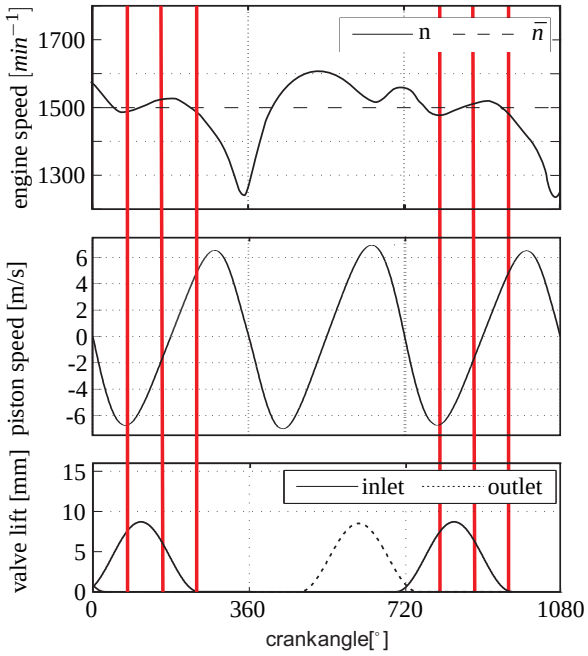

Figure 2: Progression of engine speed, piston speed, and valve lift curves. The red lines mark the location of the performed measurements.

of the PMMA-cylinder, 17 calibration planes were used to calibrate and match the viewing planes for each camera. The software interpolates linearly between different calibration planes. Therefore, a high amount of calibration planes is necessary to cancel the strong radial distortion produced by the perspex liner. The seventeen different calibration planes assure a calibration for the whole volume of the measurement field. The light band was formed by an expanding and collimating lens. A rectangular aperture was used to limit the illuminated volume. The setup leads to a measurement volume with an area of 60 *mm*x60 *mm* whereas the height depends on the measuret crank angle. A programmable timing unit (PTU, LaVision) was used to obtain 300 phase-locked TPIV images at selected CAD during intake and compression (fig. 2).

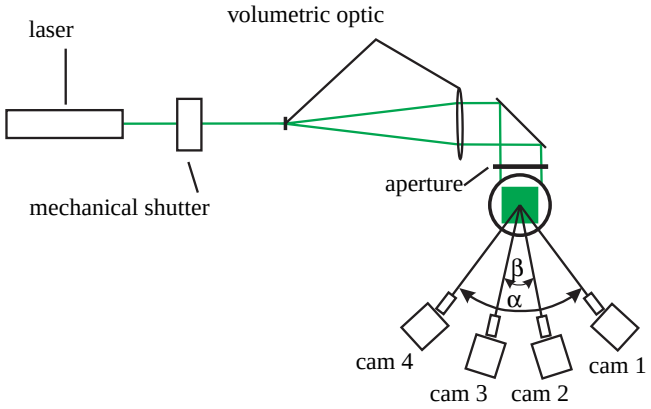

Figure 3: Tomographic PIV setup.

2.3 Tomographic preprocessing

The commercial software DaVis 8.14 (LaVision) was used to process the raw data. Before the volume reconstruction was performed, a 5x5 sliding minimum was subtracted from the raw images to remove background noise. Additionally, a 3x3 gaussian smoothing was applied to further improve the image quality. A transformation matrix (3^{rd} order polynominal approach) based on the images of the seventeen calibration planes was used to match the viewing planes of all four cameras. Subsequently, several volume self-calibration steps were applied for the different measured crank angles to further reduce the deviation of the 3^{rd} order polynominal approach leading to a remaining deviation of less than 0.2 pixels.

2.4 PIV (post-)processing

The volumetric reconstruction was performed with an iterative multiplicative algebraic reconstruction technique (fast-MART, Davis 8.14, LaVision) with an average particle density of 0.03 particles per pixel (ppp). For volume reconstruction the algorithm uses 5 iteration steps with smoothing between each step. A multi-pass direct correlation with decreasing window size and a final step of 96x96x96 voxel^3 was used, to calculate the velocity fields. The data was calculated with 75% overlap which results in a vector spacing of 0.85 mm. A 5x5x5 vector universal outlier detection was used after each correlation step to detect spurious vectors (Westerweel et al. [22]). The flow field was then smoothed with a 3x3x3 gaussian smoothing algorithm. In the final step, the same universal outlier detection was used, whereas the smoothing was skiped. The Tomo-PIV post-processing was done using Matlab (The Mathwork Inc.). The ensemble-averaged velocity, the turbulent kinetic energy (TKE), and the Γ_1-criterion were calculated to analyze the velocity fields. The ensemble-averaged mean velocity component in the x-direction $\overline{u}$ is defined by

$$\overline{u} = \frac{1}{n}\sum_{i=1}^{n} u_i \quad , \tag{1}$$

where u represents the velocity and l the number of vector fields for the defined crank angle. The averaged variance $\overline{u'^2}$ is defined by

$$\overline{u'^2} = \sigma_u^2 = \frac{1}{n}\sum_{i=1}^{n} u_i'^2 = \frac{1}{n}\sum_{i=1}^{n} (u_i - \overline{u})^2 \quad , \tag{2}$$

with u' being the velocity fluctuation and σ_u the standard deviation of u. Note that the overall velocity fluctuations result from cyclic variations on the one hand and the turbulent fluctuations. The turbulent kinetic energy (TKE) is computed by

$$k = \frac{1}{2}(\overline{u'^2} + \overline{v'^2} + \overline{w'^2}) \quad . \tag{3}$$

According to Dannemann et al. [8], the TKE possesses an uncertainty range due to the fact that it also includes the cyclic variations. Nevertheless, the qualitative character of the TKE can be described by k.
To visualize the vortical structures, the Γ_1-criterion (Graftieaux et al. [9]) was calculated

$$\Gamma_1 = \frac{1}{s}\sum_{i=1}^{s} \frac{s \times v}{||r||\,||v||} \tag{4}$$

were, s represents the number of grid points used to calculate Γ_1, r is the radius vector, and v the velocity vector at point i.

2.5 Tracer particles

Due to too low a light intensity particles with better light scattering behavior than the standard Di-Ethyl-Hexyl-Sebacat (DEHS) droplets with a diameter of 0.5 - 1 μm are required. Therefore, Expancel Microspheres (MS) with a mean diameter of about 40 μm and a density of 25 kg/m^3 were used. To ensure that the flow following behavior of the particles is sufficient, the relaxation time τ, described by Ruck et al. [15]

$$\tau = \frac{2}{9}\frac{r^2 \rho_p}{\nu \rho_f} \tag{5}$$

was calculated. The quantity r is the radius of the particle, ρ_p the density of the particle, and ρ_f the density of the fluid. With the values given above, the relaxation time was $\tau = 119.35\ \mu s$, whereas DEHS possesses a relaxation time of about $\tau = 3\ \mu s$. Hence, a Stokes number S_k can be calculated for both particles (Tropea et al. [19])

$$S_k = \frac{u_f \cdot \tau}{l_f} \quad , \tag{6}$$

where u_f is a characteristic flow velocity and l_f a characteristic flow length scale. Tropea et al. [19] state that the condition $S_k \leq 0.1$ yields an acceptable flow tracing accuracy with errors below 1%. Assuming a maximum flow velocity of about 20 m/s (Dannemann et al. [8] and integral length scales of about 3.5 mm (Petersen and Ghandi [13]), the Stokes number for Microspheres (MS) can be calculated to $S_{k,MS} = 0.5634$ (Stokes number for DEHS: $S_{k,DEHS} = 0.0435$). These analytical results lead to the assumption that Microspheres might not be appropiate for measurements in IC enginges. Hence, two component PIV measurements with both kinds of particles (MS and DEHS) where performed to analyze the flow following behavior in more detail. The velocity fields were used to calculate the energy spectra for both measurements at a given point ([x,z] = (0 mm, 50 mm)), see fig 4. For both particles, the spectrum of the initial subrange is well captured. Furthermore, both energy spectra show good agreement. With this, despite the fact that the analytical results are not satisfactory, one can assume that MS are fitted for Tomographic PIV measurements of the large scale structures (integral lenght scale) of the flow field inside an IC engine. For measurements of smaller turbulent structures, i.e., in the range of Taylor length scales, MS seem to be unapt, concerning their flow following behavior.

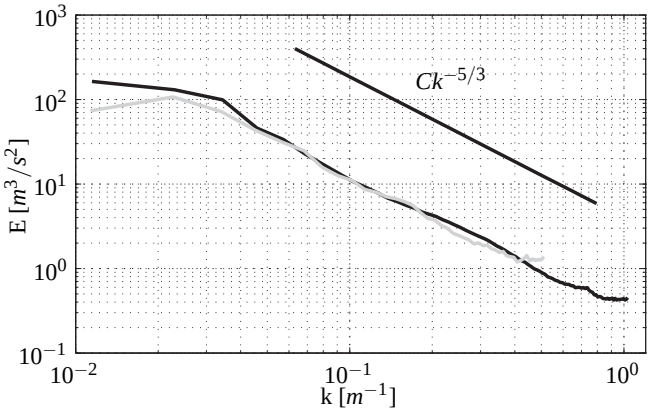

Figure 4: Energy spectra at a crank angle of 160 atdc obtaineed 2C-PIV measurements with DEHS (black) and MS (grey)

3. RESULTS AND DISCUSSION

In the following, the measured flow fields are described in detail. In the first subsection, an estimate of the measurement errors is given to assess the reliability of the results. Subsequently, the ensemble averaged velocity fields of the different CA's are described in detail using a three-dimensional visualization of the flow.

3.1 Error Estimate

The quality of PIV measurements can be assessed by applying the mass conservation principle (Zhang et al [23]). Assuming a spatial uniform density, the mass conservation can be written as

$$\frac{\partial \rho}{\partial t} + \frac{\partial(\rho u_i)}{\partial x_i} = 0. \tag{7}$$

Since density gradients can be assumed nearly zero in the recording time, the continuity equation can be approximated by

$$\frac{\partial u_i}{\partial x_i} = 0 \tag{8}$$

Non-zero values of the divergence indicate an uncertainty of the measurement results. Figure 5 shows the propability density function (PDF) of the divergence for the different CA's. It is evident that the PDF at 80° atdc is skewed in positive direction and slightly shifted to negative ΓU values. The broadening is due to the higher overall velocity during the intake, whereas the shifting evidences a not fully converged measurement. The increasing value of the PDF for 160° atdc and 240°

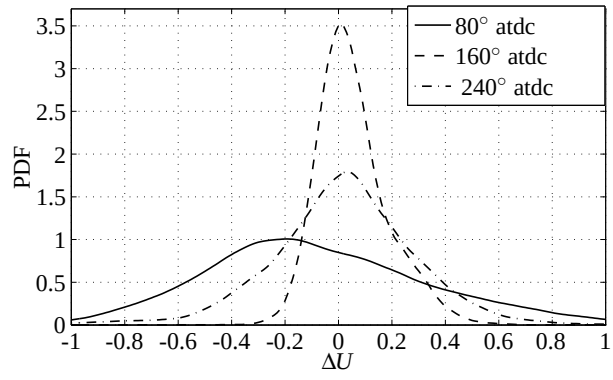

Figure 5: PDF of velocity flux for intake (80° atdc and 160° atdc) and compression (240° atdc)

atdc shows the decelerating nature of the flow field and therefore a higher PDF value for zero divergence.
The standard deviation of the normalized velocity flux

$$\sigma = \sqrt{\frac{1}{N-1}\sum_{CV}\left(\frac{\Delta U(CV)}{U_{av}(CV)} - \frac{1}{N}\sum_{CV}\frac{\Delta U(CV)}{U_{av}(CV)}\right)^2} \tag{9}$$

was calculated to show the validity of the data. Here, U_{av} is the averaged velocity vector that enters a control volume (CV). Table 1 shows the values for the different CA's. The precision uncertainty for 240° is 6.94% and increases up to 18.95% for 80° atdc. Apart from the 80° measurements, the values are in good agreement with other tomographic measurements (Baum et al. [2], Scarano and Poelma [16]). As for 80° atdc the higher uncertainty results out of higher velocities and the inability to resolve the volumetric velocity at the given resolution. The effect of the distortion of the Perspex liner can be assumed to be a systematic error for all measurements.

Table 1: Standard deviation of the normalized velocity flux for the different crank angles

$^\circ atdc$	σ [%]
80	18.95
160	9.65
240	6.94

3.2 Three-Dimensional Flow Results

To visualize the ensemble-averaged flow fields of the three different crank angles, fig. 6 and fig. 7 show one x-z plane (y = 0 mm), and two y-z planes (x = 29.5 mm and x = -8.5 mm) color-coded with the turbulent kinetic energy k, two-dimensional surface lines on the x-z plane (black), instantaneous streamlines of the three-dimensional flow (red) and isocontours of the Γ_1-criterion (blue) with respect to the x-axis. To keep the focus onto the main flow details, only one half of the engine flow field clearly is shown, since it is nearly symmetric with respect to the tumble plane.
The flow field of 80° atdc, fig. 6, shows a strong jet between the inlet valves. Furthermore, the turbulent kinetic energy shows high values in the upper region of the cylinder between the inlet valves. The blue isocontour shows the propagation of one half of a vortex ring that forms under the inlet valves. This ring vortex possesses an elongated shape which is due to the strong inlet velocity beneath the inlet valves. The irregular structure of the isocontour evidences that the vortex ring is not yet fully developed. The tumble vortex that is typical for this engine is not jet formed. This is due to the not specially for tumble flow developed inlet ports (Boree and Miles [4]).

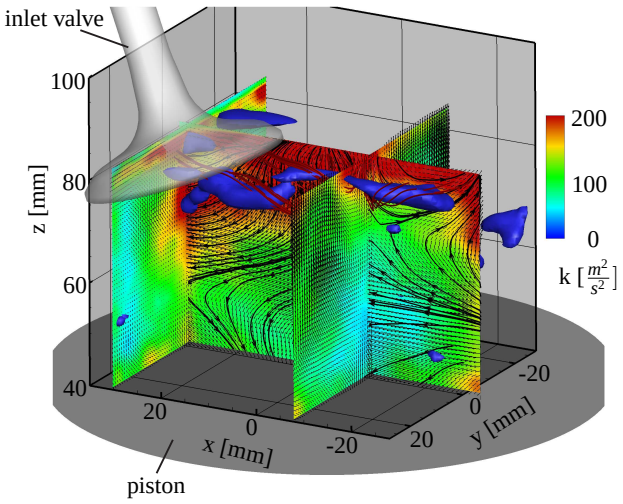

Figure 6: Three-dimensional visualization of the engine flow at 80° atdc. Streamlines (red), surface lines (black), isocontours of Γ_1 criterion (blue), and turbulent kinetic energy (color code of the different planes) are shown.

Figure 7a shows the flow field at 160° atdc. The ring vortex is fully developed, which can be seen at the Γ_1-isocontour. The streamlines furthermore show the propagation of the vortex. Due to the still open inlet valves, the flow possesses a strong downward velocity component resulting, in a now fully developed tumble vortex. This vortex can be seen by the surface lines (black) in the x-z plane. in the lower part of the flow field. A second Γ_1-isocontour shows a second counter-rotating vortex pair. This vortex pair results of the roll-up of the flow at the cylinder walls and contributes to the turbulent structure of the flow. Compared to 80° atdc, the absolute value of TKE is decreased by a factor of 10 but the highest values can still be found in the upper part of the cylinder between the inlet valves. The lowest values are in the region of the tumble vortex.
Figure7b shows the flow field at 240° atdc. The ring vortex begins to collapse. No new energy is transfered in the rotational energy due to the now missing inlet jet. Therefore, the vortex ring broadens. This can also be seen at the streamlines around the Γ_1-isocontour. The tumble vortex is outside the measurement area but can still partly be seen through the surface lines in the lower left part of the x-z plane. The lower part of the flow field possesses an upward flow component resulting out of the piston movement. The TKE is further reduced. High values can only be found at the borders of the measurement section.

4. CONCLUSION

Tomographic particle-image velocimetry (Tomo-PIV) measurements have been conducted in the cylinder of a four-valve internal combustion (IC) engine at 80°, 160°, and 240° atdc. The resolved measurement volume has a size of about 60 x 60 x 80 mm^3 for the 160° atdc measurements, whereas the height decreases for the other crank angles. This leads with an vector spacing of 0.85 mm to approximately 450,000 vectors for measurements at 160° atdc. For all crank angles, the ensemble-averaged velocity fields and the turbulent kinetic energy (TKE) have been determined using 300 instantaneous vector fields. An error estimate, based on the mass conservation principle has shown that the error is in the same order of magnitude as volumetric flow measurements conducted in generic

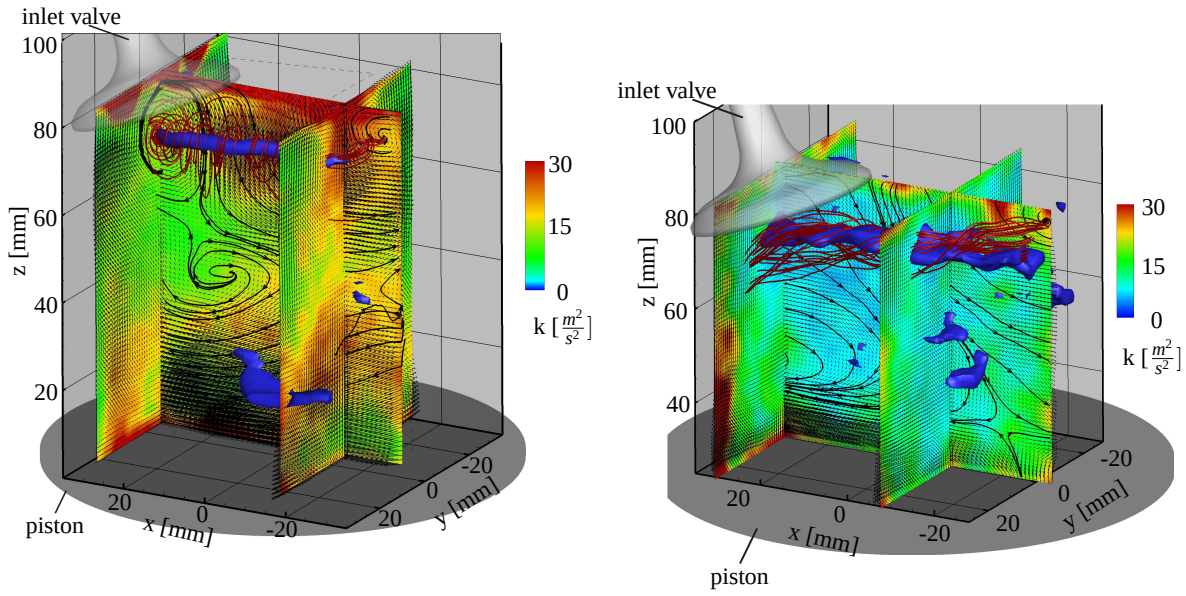

(a) 160° atdc (b) 240° atdc

Figure 7: Three-dimensional visualization of the engine flow at 160° and 240° atdc. Streamlines (red), surface lines (black), isocontours of Γ_1 criterion (blue), and turbulent kinetic energy (color code of the different planes) are shown.

configurations. The volumetric analysis of the flow fields shows the propagation of the inlet vortices which form a vortex ring as well as the tumble vortex. Future investigations will focus on measuring other configurations and crank angles.

REFERENCES

[1] P. Adomeit, A. Sehr, R. Weinowski, K. G. Stapf, D. Seebach, S. Pischinger, K. Hoffmann, D. Abel, F. Fricke, H. Kleeberg, and D. Tomazic. Operation strategies for Controlled Auto Ignition CAI Engines. In *SAE World Congress*, Detroit, MI, USA, April 2009. SAE Paper No. 2009-01-0300.

[2] E. Baum, B. Peterson, Ch. Surmann, D. Michaelis, B. Böhm, and A. Dreizler. Tomographic PIV measurements in an IC engine. In *16th Int Symp on Applications of Laser Techniques to Fluid Mechanics, Lisbon, Portugal,*, 2012.

[3] A. Bhave, M. Kraft, F. Mauss, A. Oakley, and H. Zhao. Evaluating the EGR-AFR Operating Range of a HCCI Engine. In *SP-1963 Homogeneous Charge Compression Ignition (HCCI) Combustion 2005*, 2005.

[4] J. Boree and P. C. Miles. In-cylinder flow. In *Accepted for publication in Encyclopedia of Automotive Engineering*. John Wiley & Sons, Ltd., 2013.

[5] I. Bücker, D. Karhoff, M. Klaas, and W. Schröder. Stereo-PIV Measurements of the In-Cylinder Flow of a Motored Four-Valve Combustion Engine. In *9th Int. Symp. on Particle-Image Velocimetry - PIV11 Kobe, Japan*, 2011.

[6] I. Bücker, D. Karhoff, M. Klaas, and W. Schröder. Stereoscopic Multi-Planar PIV Measurements of In-Cylinder Tumbling Flow. *to be published to Exp Fluids*, Online first: DOI:10.1007/s00348-012-1402-5, 2012.

[7] P. Calendini, T. Lecerf, and M. Trinite. In cylinder velocity measurements with stereoscopic particle image velocimetry in a SI engine. *SAE 2000.01.1798*, 01, 2000.

[8] J. Dannemann, K. Pielhop, M. Klaas, and W. Schröder. Cycle resolved multi-planar flow measurements in a four-valve combustion engine. *Exp Fluids*, 50:961976, 2010. Online First.

[9] L. Graftieaux, M. Michard, and N. Grosjean. Combining PIV, POD and vortex identification algorithms for the study of unsteady turbulent swirling flows. *Measurement Science and Technology*, 12:1422–1429, 2001.

[10] R. Konrath, W. Schröder, and W. Limberg. Holographic particle-image velocimetry applied to the flow within the cylinder of a four-valve internal combustion engine. *Exp Fluids*, 33:781–793, 2002.

[11] O. Lang, W. Salber, J. Hahn, S. Pischinger, K. Hortmann, and C. Buecker. Thermodynamical and Mechanical Approach Towards a Variable Valve Train for the Controlled Auto Ignition Combustion Process. *SAE Paper*, 01-0762, 2005.

[12] T. Ma, H. Zhao, J. Li, and N. Ladommatos. Experimental Investigation of Controlled Auto-ignition (CAI) Combustion in a 4-stroke Multi-Cylinder Gasoline Engine And Drive Cycle Simulations. *A new Generation of Engine Combustion Processes for the Future*, pages 115–124, 2001.

[13] B. Petersen and J. Ghandhi. High-resolution turbulent scalar field measurement in an optically accessible internal combustion engine. *Exp Fluids*, 51:1695–1708, 2011.

[14] M. Reeves, D.P. Towers, B. Tavender, and C.H. Buckberry. A high-speed all-digital technique for cycle-resolved 2-D fow measurement and fow visualisation within SI engine cylinders. *Optics and Lasers in Engineering*, 31:247–261, 1999.

[15] B. Ruck. Einfluß der Tracerteilchengröße auf die Signalinformation in der Laser-Doppler-Anemometrie. *Technisches Messen*, 57:284–295, 1990.

[16] F. Scarano and C. Poelma. Three-dimensional vorticity patterns of cylinder wakes. *Exp Fluids*, 47:69–83, 2009.

[17] P. Stansfield, G. Wigley, T. Justham, J. Catto, and G. Pitcher. PIV analysis of in-cylinder flow structures over a range of realistic engine speeds. *Exp Fluids*, 43:135–146, 2007.

[18] K.G. Stapf, D. Seebach, F. Fricke, S. Pischinger, K. Hoffmann, and D. Abel. CAI-Engines: Modern combustion system to face future challenges. In *SIA Int. Conference - The Spark Ignition Engine of the Future*, Strasbourg, November 2007.

[19] C. Tropea, A. Yarin, and J. Foss. *Handbook of Experimental Fluid Mechanics*. Springer, Berlin, 2007.

[20] T. Urushihara, K. Hiraya, A. Kakuhou, and T. Itoh. Parametric Study of Gasoline HCCI with Various Compression Ratios, Intake Pressures and Temperatures. In *IFP International Congress*, Rueil-Malmaison, 2001.

[21] T. van Overbrüggen, J. Dannemann, M. Klaas, and W. Schröder. Holographic particle-image velocimetry measurements in a four-valve combustion engine. *accepted for publication Exp Fluids*, 2012.

[22] J. Westerweel. Efficient detection of spurious vectors in particle image velocimetry data. *Exp*, 45:549–556, 1994.

[23] J. Zhang, B. Tao, and J. Katz. Turbulent flow measurement in a square duct with hybrid holographic PIV. *Exp Fluids*, 23:373–381, 1997.